NASA Technical Paper 1028

Aerodynamic and Directional Acoustic Performance of a Scoop Inlet

John M. Abbott and Donald A. Dietrich

SEPTEMBER 1977

NASA

NASA Technical Paper 1028

Aerodynamic and Directional Acoustic Performance of a Scoop Inlet

John M. Abbott and Donald A. Dietrich

Lewis Research Center
Cleveland, Ohio

National Aeronautics
and Space Administration

**Scientific and Technical
Information Office**

1977

AERODYNAMIC AND DIRECTIONAL ACOUSTIC PERFORMANCE OF A SCOOP INLET

by John M. Abbott and Donald A. Dietrich

Lewis Research Center

SUMMARY

A series of tests was conducted to determine the aerodynamic and directional acoustic performance of a scoop inlet. The scoop inlet is designed with a portion of the lower cowling extended forward to direct upward any noise that is propagating out the front of the engine toward the ground.

The tests were conducted in the Lewis anechoic wind-tunnel facility at free-stream velocities of 0, 18, 41, and 61 meters per second and angles of attack from -10° to 120°. The inlet throat Mach number was varied from 0.30 to 0.75.

Aerodynamically, at a free-stream velocity of 41 meters per second, the design throat Mach number (0.63), and an angle of attack of 50°, the scoop inlet total-pressure recovery was 0.989 and the total-pressure distortion was 0.15. The angles of attack where flow separation occurred with the scoop inlet were higher than those for a conventional symmetric inlet.

Acoustically, the scoop inlet provided a maximum noise reduction of 12 to 15 decibels below the inlet over the entire range of throat Mach number and angle of attack at a free-stream velocity of 41 meters per second.

INTRODUCTION

Inlet-radiated fan noise has traditionally been reduced by using one of two suppression techniques: (1) surface acoustical treatment with or without inlet duct splitters (ref. 1), and (2) sonic inlets (refs. 2 and 3). Both methods, however, have certain disadvantages. For example, significantly reducing noise with surface acoustical treatment may require considerable increases in inlet length (for more treated area), with corresponding increases in weight, total-pressure loss, and ultimately airplane operating cost. Inlet splitters cause additional performance losses and are generally

disliked by aircraft engine users. The main disadvantage of the sonic inlet is the complicated variable geometry required to provide sonic flow in the inlet throat at both takeoff and approach engine flow settings.

A different approach to the problem of reducing inlet noise is not to suppress the inlet-radiated noise but to change the directivity of the propagating noise, that is, direct upward the noise that normally would be propagating toward the ground. This redirection technique has been explored extensively in regard to shielding engine rear noise from the ground by using an over-the-wing engine installation. Here the upper surface of the aircraft wing serves to direct the rear noise upward (ref. 4). In a similar manner, an inlet with a portion of the lower cowling extended forward, that is, a scoop inlet, can serve to direct upward any noise that would normally propagate out the front of the engine toward the ground. In the case of a scoop inlet, the noise redirection is due to a combination of upward reflection from the extended lower lip and upward refraction from the inflow velocity gradients generated within the scoop inlet duct. The aeroacoustic performance of such a scoop inlet is the subject of the experimental results reported herein.

The potential advantage of the scoop inlet over the sonic inlet is obvious - a variable-geometry system is not required. The passive scoop inlet would work equally well at takeoff and approach engine flow settings. Compared with the treated inlet, it should be possible to attain the same noise reduction with the shorter, lighter, and structurally simpler scoop inlet. The asymmetric shape of the scoop inlet, however, makes the aerodynamic design of the inlet more difficult than for a conventional axisymmetric inlet. This is particularly true for the cruise condition, where the external forebody of the inlet needs to be designed to accommodate an asymmetric flow spillage.

The investigation described herein was conducted to determine the low-speed (takeoff and approach) aerodynamic and directional acoustic performance of such a scoop inlet. The 30.48-centimeter-diffuser-exit-diameter scoop inlet was tested in the Lewis anechoic wind tunnel facility along with a baseline, or conventional, inlet. Data were taken at free-stream velocities of 0, 18, 41, and 61 meters per second; angles of attack from -10° to 120°; and throat Mach numbers of 0.3, 0.54, 0.63 (design), 0.70, and 0.75.

SYMBOLS

a ellipse semimajor axis of internal lip (fig. 3)

b ellipse semiminor axis of internal lip (fig. 3)

D diameter

D_{max}	inlet total-pressure distortion parameter, (Maximum total pressure) - (Minimum total pressure)/(Average total pressure)
f_f	1/3-octave filter center frequency
f_s	siren frequency
H	passage height at diffuser exit (fig. 3)
h	radial distance from tip at diffuser exit (fig. 3)
L	length
M	Mach number
P	total pressure
p	static pressure
ΔSPL	sound pressure level reduction, (Baseline inlet sound pressure level) - (Scoop inlet sound pressure level), at same conditions of free-stream velocity, angle of attack, and throat Mach number
V	velocity
X	external forebody length (fig. 3)
x	axial distance from inlet highlight (fig. 3)
Y	external forebody thickness (fig. 3)
y	radial distance from inlet highlight (fig. 3)
α	angle of attack, deg
β	microphone orientation angle, deg
λ_{max}	maximum diffuser wall angle (fig. 3), deg
χ	external forebody length (fig. 3)
ψ	inlet circumferential position (fig. 3), deg

Subscripts:

av	average
c	centerbody
d	diffuser
e	diffuser exit
hl	inlet highlight
max	maximum

s	inlet surface
sep	flow separation
t	inlet throat
0	free stream
1	rake measuring station (simulated fan face)

APPARATUS

Test Installation

The tests were conducted in the Lewis 2.74- by 4.58-meter (9- by 15-ft) anechoic wind tunnel facility (ref. 5). A vacuum system was used in place of a fan or compressor to induce inlet flow. A schematic view of the test installation and facility is shown in figure 1.

A venturi, calibrated in place against a standard ASME bellmouth whose flow measurement had been corrected for boundary layer growth, was used to measure inlet airflow. The scatter in the airflow calibration data was approximately ±0.2 percent at a nominal weight flow of 11.68 kilograms per second. Inlet airflow was remotely varied by using two butterfly valves arranged to give both coarse and fine adjustment. Inlet angle of attack was remotely varied by a turntable on which the test apparatus was mounted.

To determine the acoustic properties of the test inlets with the vacuum flow system, a siren was installed in the flow duct downstream of the inlet. The siren was a 13.97-centimeter-diameter, single-stage fan modified by the addition of struts and a screen just upstream of the rotor to increase its noise level. The siren was located approximately three inlet diameters downstream of the simulated fan face (fig. 1).

Directional noise measurements were made by using a microphone located 1.22 meters in front of the inlet face. The microphone was remotely rotated about a pivot point at the inlet face, allowing noise data to be taken in the flyover plane at various angles relative to the inlet centerline. The anechoic character of the wind tunnel, along with more details of the acoustic measurement system, is described in references 6 to 8.

The model as it appeared in the wind-tunnel test section is shown in figure 2.

Inlet Design

The major variables defining the geometry of the baseline (symmetric) inlet and the scoop inlet are shown in figure 3. Both inlets had a diffuser-exit diameter D_e of 30.48 centimeters with a design throat Mach number of 0.63. Nearly all the geometric design parameters were the same for both inlets and are listed in table I. The main difference between the two inlets, of course, was that the inlet length L was dependent on circumferential location ψ for the scoop inlet and was constant for the baseline inlet. The circumferential variation of length for the scoop inlet provided for the upward redirection of the inlet-radiated noise (through a combination of reflection and refraction) and is given in table II. Note that from circumferential positions ψ of 113.64° to 246.36°, the inlet length was constant (L/D_e of 0.716) and equal to that of the baseline inlet. Closer to the lower lip of the scoop inlet, the length became greater, through a lengthening of the inlet throat section, to a maximum L/D_e of 1.295.

As indicated in table I, the internal lip design was a 2-to-1 ellipse with a relatively high area-contraction ratio of 1.44 for good high-angle-of-attack performance in a short-takeoff-and-landing (STOL) aircraft application. The external forebody design for both inlets was selected for a cruise Mach number of 0.76 by using design charts for symmetric inlets. This design would be expected to work quite well at cruise with the symmetric baseline inlet. However, the scoop inlet, with its asymmetric spillage properties at cruise, may require a different external forebody design.

The inlet diffuser was a cubic shape with an equivalent conical half-angle of 1.33°, a maximum wall angle of 8.37°, and a ratio of diffuser length to diffuser-exit diameter L_d/D_e of 0.538. The diffuser was axisymmetric and was, in fact, the same piece of hardware for both inlets (the lips were removable). The centerbody diameter was 0.4 of the diffuser-exit diameter and was a 2-to-1 ellipse shape.

Instrumentation and Data Reduction

Aerodynamic data. - The instrumentation used to determine the aerodynamic performance of the inlets is shown in figure 4. A total of 85 internal surface static-pressure measurements were made with the scoop inlet and 69 with the baseline inlet. Section A-A of figure 4 shows the total-pressure rakes and static-pressure taps located at the rake measuring plane. Rake plane total-pressure measurements were made by using both hub and tip boundary-layer rakes as well as total-pressure rakes spanning the entire annulus. Eight full-span, total-pressure rakes were used with six equal-area-weighted tubes per rake. The hub and tip boundary-layer rakes each contained five total-pressure tubes.

Inlet total-pressure recovery $P_{1,av}/P_0$ was computed from all measured total pressures, including those from boundary-layer rakes, with the appropriate area-weighting terms. However, in computing inlet total-pressure distortion D_{max}, boundary-layer measurements taken closer to the wall than the nearest tube on the six-element, equal-area-weighted rakes were omitted. Using these rakes as a reference resulted in excluding measurements closer to the wall than 9.3 percent of the annulus area.

Inlet throat Mach number M_t was computed from the inlet flow measured by the venturi, with a correction for the high-pressure air required to drive the siren. The throat Mach number used as a parameter in presenting the data was computed from the measured weight flow and the inlet geometric throat area, assuming uniform flow.

Acoustic data. - Directional noise measurements were made with a microphone located 1.22 meters in front of the inlet face. The microphone was remotely rotated about a pivot point at the inlet face, allowing noise data to be taken in the flyover plane at various angles relative to the inlet centerline. An on-line graphic display of noise levels provided a continuous trace of 1/3-octave sound pressure level versus microphone orientation angle β as the microphone rotated. Any 1/3-octave center frequency could be selected for the trace. In addition, the microphone was positioned at fixed values of β, where magnetic tape data were recorded for later 1/3-octave spectral analysis. The noise data acquisition system in the Lewis anechoic wind tunnel is described in reference 8.

Test Procedure

The two inlets were tested at free-stream velocities of 0, 18, 41, and 61 meters per second and at angles of attack from -10° to 120°. Inlet airflow was varied to cover a range of throat Mach number from 0.31 to 0.75.

At the 18-meter-per-second free-stream velocity, tests were conducted with the scoop inlet at an angle of attack of 90° to simulate crosswinds during engine startup and ground taxi. (The inlet was rotated 90° about its axis to obtain the proper orientation.)

Data were obtained on line to determine the angle of attack where inlet flow separation occurred. This was done by monitoring a lip surface static pressure and a diffuser-exit total pressure, both on the windward side, as the angle of attack was increased from 0° to 120°. This method has been used successfully in the past and is detailed in reference 9.

Aerodynamic testing and acoustic testing were done separately. During the aerodynamic tests, the noise siren was not used. During the acoustic tests, the inlet weight flow was set at the desired value, the siren speed was adjusted to set the blade

passing frequency at 9600 hertz, and the acoustic data were taken.

The standard test procedure was to set the free-stream velocity and inlet weight flow, and to record data at discrete angles of attack. Weight flow was then changed and data were taken again at the same discrete angles of attack. Finally, free-stream velocity was changed and the procedure was repeated over the weight-flow and angle-of-attack range.

RESULTS AND DISCUSSION

Aerodynamic Performance

Basic performance. - The basic aerodynamic performance of the scoop and baseline inlets is shown in figure 5 in terms of total-pressure recovery and distortion versus throat Mach number. In figure 5(a), static performance is shown and indicates lower recoveries and higher distortions for the scoop inlet as compared with the baseline inlet over the entire range of throat Mach number. At the design throat Mach number of 0.63, the recovery and distortion were 0.985 and 0.15 for the scoop inlet and 0.025 for the baseline inlet. The reason for the lower level of aerodynamic performance for the scoop inlet becomes apparent in a later discussion of the distributions of the total pressure at the diffuser exit and the surface static pressure distributions.

At a free-stream velocity of 41 meters per second and an angle of attack of 0° (fig. 5(b)), the aerodynamic performance of the scoop inlet improved considerably over what it was at static conditions although it was still slightly lower than the baseline inlet performance. For example, at a throat Mach number of 0.63, the recovery and distortion were 0.992 and 0.045 for the scoop inlet and 0.994 and 0.006 for the baseline inlet. Reasons for this improved performance again become apparent in a later more-detailed discussion.

Figure 5(b) also shows inlet performance at an angle of attack of 50°. (The angle of attack considered to be the maximum encountered by an inlet in a STOL aircraft installation.) The relative ranking of the two inlets remains the same. At the design throat Mach number of 0.63, the scoop inlet recovery was 0.989 and the distortion was 0.15. The values for the baseline inlet were 0.993 and 0.04, respectively.

In figure 5(c) is shown the aerodynamic performance of the two inlets at a free-stream velocity of 61 meters per second and angles of attack of 0° and 50°. At 0° angle of attack, the performance of the two inlets was nearly identical to a throat Mach number between 0.63 and 0.72, where the recovery dropped and the distortion increased for the scoop inlet. Perhaps the most striking feature of figure 5(c), however, is that at a 50° angle of attack and throat Mach numbers either side of 0.54, flow sepa-

ration had occurred for the baseline inlet (as evident from the very low recoveries and high distortions) but had not occurred for the scoop inlet. It is shown in a later figure that over the full range of test conditions, the angle of attack where flow separation occurs was significantly higher for the scoop inlet than for the baseline inlet.

Distribution of total pressure in tip boundary layer. - Presented in figure 6 is the distribution of the total pressure in the tip boundary layer at four circumferential positions at the inlet diffuser exit for the scoop and baseline inlets at a throat Mach number of 0.63 (design). At static conditions (fig. 6(a)), it is apparent that the lower recoveries and higher distortions noted for the scoop inlet in figure 5(a) were a result of total-pressure losses occurring primarily at circumferential positions ψ of 112.5° and 157.5°. This is a result of higher inlet surface velocities over this circumferential extent of the scoop inlet caused by its tendency to draw more of its airflow from above. The surface static-pressure distributions to be discussed in the next section verify this.

The already noted improvement in scoop inlet recovery and distortion with free-stream velocity is evident from the tip boundary-layer distributions in figure 6(b) at a free-stream velocity of 41 meters per second and an angle of attack of 0°. The effect of the free-stream velocity was to more evenly distribute the flow coming in over the upper and lower portions of the inlet, thus reducing the losses in the upper portion.

At 50° angle of attack (fig. 6(c)), the tip boundary layer again illustrates the lower recovery and higher distortion for the scoop inlet, especially at $\psi = 112.5^{\circ}$. At 75° angle of attack (fig. 6(d)), the flow had completely separated from the lower lip of the baseline inlet, as indicated by the boundary-layer, total-pressure distribution at $\psi = 22.5^{\circ}$, while the flow was still attached to the lower lip of the scoop.

At $\psi = 112.5^{\circ}$ a rather unusual total-pressure distribution is evident for the scoop inlet, with total pressure first decreasing and then increasing as distance from the surface increased. In fact, in figures 6(a) and (c), the total-pressure distribution at this same circumferential position is also different from what would be expected for a thickened boundary layer or a flow separation. It is possible that this type of total-pressure distribution is due to a vortex that has formed in the "corner" of the scoop-side profile and is propagating back through the inlet. Because of the flow angularity resulting from the spinning vortex flow and the mean axial flow, the total-pressure probes would tend to indicate lower total pressures. (Probes of this type are typically insensitive to flow angles to about $\pm 20^{\circ}$.) And if the vortex were lifted off the inlet surface far enough, one would expect to see the type of total-pressure distribution shown in figure 6(d) at $\psi = 112.5^{\circ}$. Here the vortex core, where the flow angle would be most different from axial, was apparently off the surface at a fraction of the passage height h/H of about 0.12, where the indicated total-pressure loss was greatest. Note that away from this location, either closer to or farther from the surface, the total

pressure increased, indicating a return of the flow angle closer to axial, as would be expected when moving outward from the core of a vortex. This same phenomenon has been noted in total-pressure measurements made in studies of inlet ground vortices during reverse-thrust operation, as reported in reference 10.

In summary, the tip boundary-layer, total-pressure distributions have indicated that higher total-pressure losses tend to occur over the upper portion of the scoop inlet, where a larger percentage of the inflow occurs. The presence of free-stream velocity tends to moderate this effect. There is also evidence of vortices being formed in the "corners" of the scoop side profile, resulting in indicated values of total pressure at the diffuser exit that may be lower than those actually existing. This may mean that the indicated values of recovery are slightly too low and the values of distortion slightly too high for the scoop. But then the vortex itself is another kind of distortion that must be recognized. It is possible that a modification of the side contour (to decrease the sharpness of the "corner") may eliminate or reduce the severeness of the vortices.

Surface pressure distributions. - Shown in figure 7 is the axial distribution of static pressure in the baseline inlet at $\psi = 0^{\circ}$ and in the scoop inlet at ψ of 0°, 90° (diffuser only), 100° (lip only), and 180°. The data are plotted as the ratio of surface static pressure to free-stream total pressure versus axial distance as measured downstream of the scoop highlight at $\psi = 0^{\circ}$. At static conditions (fig. 7(a)), the higher surface velocities over the upper portion of the scoop inlet are evident from the low values of static pressure at ψ of 100° and 180°, which correspond to supersonic surface Mach numbers to about 1.35. Note that the flow velocities over the lower extended lip of the scoop ($\psi = 0^{\circ}$) are by comparison quite small. The higher surface velocities over the upper portion of the scoop are what account for the lower recovery and higher distortion of the scoop at static conditions.

As can be seen in figure 7(b), a free-stream velocity of 41 meters per second at an angle of attack of 0° tended to redistribute the incoming flow in the scoop by lowering the velocities on the upper portion of the inlet and just slightly increasing them on the lower portion. In going from static conditions to a free-stream velocity of 41 meters per second, the minimum surface pressure ratio (maximum velocity) at $\psi = 100^{\circ}$ increased (velocity decreased) from 0.335 to 0.490. This accounts for the improved levels of recovery and distortion resulting from free-stream velocity.

Increasing the angle of attack to 50° (fig. 7(c)) resulted in a large decrease in surface static pressure (increase in surface Mach number to about 1.43) on the lower lip ($\psi = 0^{\circ}$) of the baseline inlet, while the lower lip of the scoop inlet has very modest surface velocities. It appears that the $\psi = 100^{\circ}$ position (near the "corner") is the most critical region in terms of high surface velocities with the scoop inlet as angle of attack is increased. Also, with the scoop inlet there was no evidence in the surface

pressure distribution of any flow separation. This tends to support the conjecture that the indicated tip boundary-layer, total-pressure distribution at $\psi = 112.5^{\circ}$ in figure 6(c) was due to the presence of a vortex.

At 75° angle of attack (fig. 7(d)), the flow separation with the baseline inlet is evident from the flat axial distribution of static pressure. There still appears to be no evidence of flow separation from the scoop at any circumferential position. The static pressure on the lower lip at the highlight had dropped considerably, but the lowest value of static pressure still occurred at $\psi = 100^{\circ}$.

The variation in the amount of flow that is entering the scoop at different circumferential positions is indicated by the circumferential variation in surface static pressure at the inlet highlight for the scoop and baseline inlets, as shown in figure 8. At a free-stream velocity of 41 meters per second, an angle of attack of 0°, and a throat Mach number of 0.63, the static-pressure distribution around the highlight of the baseline inlet was almost flat. This indicates uniform inflow around the circumference. However, the distribution for the scoop inlet indicates relatively low amounts of inflow from ψ of 0° to 60° with a transition to relatively high amounts of inflow from ψ of 100° to 180°. The conclusion is that the scoop inlet tends to pull its airflow from above. At 50° angle of attack (fig. 8(b)), the lower lip of the baseline inlet, $\psi = 0^{\circ}$, had very high surface velocities and the upper lip, $\psi = 180^{\circ}$, very low. On the other hand, the surface velocities at the highlight over the lower lip of the scoop were not nearly as high as the baseline. However, note that, at $\psi = 100^{\circ}$ on the scoop, the surface velocity is approaching that of the lower lip of the baseline inlet. This points out again that the "corner" in the side contour of this scoop inlet design may be the most critical area and that an improvement in its design may well result in significant aerodynamic performance improvements.

Flow separation bounds. - The flow separation bounds for the scoop and baseline inlets are given in figure 9. As previously noted, these bounds were obtained by monitoring a lip static pressure and a diffuser-exit total pressure on the windward side of the inlet as the angle of attack was steadily increased (the method is detailed in ref. 9). The data are plotted as the angle of attack where flow separation occurred versus throat Mach number at free-stream velocities of 41 and 61 meters per second. Below the bound the flow was attached; above the bound, it was separated at the lip. At 41 meters per second (fig. 9(a)), the separation bound for the scoop inlet was from 7° to 15° higher than that for the baseline inlet. At the design throat Mach number of 0.63, the flow separation angle for the baseline inlet was 71° and that for the scoop inlet was 84°. At a free-stream velocity of 61 meters per second (fig. 9(b)), the same trend is evident, with the spread in flow separation angle being between 5° and 10°.

To reiterate, the higher flow separation angles attainable with the scoop inlet are a result of the natural tendency of the incoming flow to be drawn from above, thus re-

ducing the surface velocities on the critical lower lip. And again, the critical region with this particular scoop inlet may be the side "corner," which, if made less severe, could result in even higher flow separation angles.

90° Crosswind performance. - The aerodynamic performance of the scoop inlet in a 90°, 18-meter-per-second (35-knot) crosswind is shown in figure 10 at the design throat Mach number of 0.63. The results were similar over the full throat Mach number range. The distribution of total pressure at the inlet diffuser exit (fig. 10(a)) indicates a poor level of scoop performance in a 90° crosswind. The initial suspicion might be that the flow had separated from the side of the inlet. However, the axial surface static-pressure distributions of figure 10(b) do not indicate the presence of any flow separation at circumferential angles of 0°, 45°, 60°, 90°, or 100°. What probably happened was that a vortex formed in the "corner" of the side profile, resulting in the indicated low total pressures because of excessive flow angularity into the total-pressure probes. A modified side contour may eliminate or reduce the severeness of this vortex.

Acoustic Performance

Comparison of scoop and baseline inlets. - Shown in figure 11 are typical on-line directional noise traces obtained by rotating the microphone through an orientation angle β from -110° to $+110^{\circ}$. (Negative angles are below the inlets; positive angles above.) Traces are shown for the scoop and baseline inlets at a free-stream velocity of 41 meters per second, an angle of attack of 0°, and the design throat Mach number of 0.63. The siren speed was adjusted so that the blade passing frequency was 9600 hertz. The acoustic traces for the two inlets represent the sound pressure level in the 8000-hertz-center-frequency, 1/3-octave band. A third trace, at the same frequency, is shown in the figure and represents the background level in the anechoic wind tunnel obtained at a free-stream velocity of 41 meters per second with the siren turned off and no flow through the inlet.

Traces were also taken in the 10 000-hertz, 1/3-octave band containing the siren blade passing tone. The conclusions made regarding the 8000-hertz data also apply to the 10 000-hertz data. The traces taken in the 10 000-hertz, 1/3-octave band, however, generally had a wider variation in sound pressure level at a given microphone orientation angle than had the 8000-hertz data, suggesting a time unsteadiness in the siren blade passing tone.

The data of figure 11 show that the scoop inlet indeed reduced the amount of noise that would normally propagate toward the ground, as indicated by a comparison with the noise levels for the baseline inlet at negative values of β. The amount of noise

reduction relative to the baseline inlet, designated as ΔSPL in the figure, was a maximum of about 15 decibels at a microphone orientation angle of -80° and was still about 5 decibels along the inlet centerline ($\beta = 0^{\circ}$). Even for positive β (above the inlet), the sound pressure level of the scoop inlet was lower than that of the baseline inlet. This somewhat surprising effect at positive β was probably the result of high flow Mach number suppression in the upper portion of the inlet duct as a result of the incoming flow asymmetry (refer to the discussion of fig. 8(a)). The high Mach number suppression principle is discussed in detail in reference 3.

Figure 12 shows the entire 1/3-octave spectra for the scoop and baseline inlets and the background noise at a fixed microphone orientation angle of -60°. All the test conditions are identical to those in figure 11. The spectra indicate that the scoop inlet provided a substantial level of noise reduction, ΔSPL, over the range of frequency where the background noise level is not an interfering factor ($\gtrsim$2000 Hz). Noise reductions ranged from 8 decibels at 2000 hertz to 12.5 decibels at 20 000 hertz.

Effect of throat Mach number. - Figure 13 shows the effect of inlet throat Mach number on the noise reduction ΔSPL of the scoop inlet as a function of microphone orientation angle at a free-stream velocity of 41 meters per second and an angle of attack of 0°. The ΔSPL at each microphone orientation angle was obtained by subtracting the noise level of the scoop inlet from that of the baseline inlet with both inlets operating at the exact same conditions of free-stream velocity, throat Mach number, angle of attack, and siren speed. The data indicate that over the range of throat Mach number from 0.31 to 0.70, the scoop inlet effectively reduced noise below the inlet, with maximum noise reductions of the order of 15 decibels. No systematic effect of throat Mach number was apparent below the inlet (negative β); however, there was a systematic increase in noise reduction above the inlet with increasing Mach number. This again resulted from the progressive effect of the increasing high Mach number suppression in the upper portion of the scoop inlet, which is due to the flow asymmetry in the inlet duct. Recall from figure 7 that local surface velocities were supersonic.

Effect of angle of attack. - The effect of angle of attack on the noise reduction directivity of the scoop inlet relative to the baseline inlet is shown in figure 14 for angles of attack of 0°, 15°, and 30° at a free-stream velocity of 41 meters per second and the design throat Mach number of 0.63. The data for angles of attack of 0° and 15° were nearly the same. At a 30° angle of attack, there appeared to be a slight decrease in the amount of noise reduction provided by the scoop inlet over the full range of microphone orientation angle. However, it was at most a 4-decibel loss in noise reduction, relative to the 0° angle of attack data at a microphone orientation angle of -90°; more typically, it was of the order of 1 to 2 decibels over most of the range of microphone orientation angle.

The effect of angle of attack on the baseline inlet sound pressure level is shown in

figure 15. The data indicate a progressive increase in noise level below the inlet and a decrease in level above the inlet as angle of attack was increased. This effect was probably the result of a downward (negative β) refraction of the inlet-radiated noise due to the velocity gradients generated within the inlet duct at angle of attack. Similar results are reported in reference 8. These same results were found with the scoop inlet and were even more pronounced at an angle of attack of 30°, as indicated by the drop in scoop inlet noise reduction shown in figure 14.

SUMMARY OF RESULTS

Wind tunnel tests were conducted to determine the aerodynamic and acoustic performance of a scoop inlet. Compared with an axisymmetric baseline inlet, the scoop inlet generated higher velocities in the vicinity of the upper lip and lower velocities about the lower lip. This accounts for most of the following results:

1. At static conditions and the design throat Mach number (0.63), the scoop inlet had a total-pressure recovery of 0.985 and a distortion of 0.15, as compared with respective values of 0.993 and 0.025 for the baseline inlet.

2. The aerodynamic performance of the scoop inlet improved considerably with increasing free-stream velocity. At a free-stream velocity of 41 meters per second, the design throat Mach number of 0.63, and an angle of attack of 0°, the inlet recovery was 0.992 and the distortion was 0.045. Increasing the angle of attack to 50° at these same flow conditions resulted in a recovery of 0.989 and a distortion of 0.15.

3. The flow-separation angles of attack for the scoop inlet were higher than those for the baseline inlet. For example, at a free-stream velocity of 41 meters per second and the design throat Mach number of 0.63, internal flow separation occurred at angles of attack of 71° for the baseline inlet and 84° for the scoop inlet.

4. At many of the conditions tested, there appeared to be a tendency for vortices to form in the "corners" of the scoop side profile. This was most evident in an 18-meter-per-second, 90° crosswind. An appropriate modification to reduce the severeness of the "corner" may eliminate the problem.

5. Acoustically, the scoop inlet provided a maximum noise reduction of 12 to 15 decibels below the inlet over the entire range of throat Mach number (0.31 to 0.70) and angle of attack (0° to 30°) at a free-stream velocity of 41 meters per second. The noise reduction occurred from 2000 to 20 000 hertz.

Lewis Research Center,
National Aeronautics and Space Administration,
Cleveland, Ohio, May 5, 1977,
511-54.

REFERENCES

1. Aircraft Engine Noise Reduction. NASA SP-311, 1972.
2. Abbott, J. M.: Aeroacoustic Performance of Scale Model Sonic Inlets. AIAA Paper 75-202, Jan. 1975.
3. Miller, B. A.: Experimentally Determined Aeroacoustic Performance and Control of Several Sonic Inlets. AIAA Paper 75-1184, Sept.-Oct. 1975.
4. Aeronautical Propulsion. NASA SP-381, 1975.
5. Yuska, Joseph A.; Diedrich, James H.; and Clough, Nestor: Lewis 9- by 15-Foot V/STOL Wind Tunnel. NASA TM X-2305, 1971.
6. Rentz, Peter E.: Softwall Acoustical Characteristics and Measurement Capabilities of the NASA Lewis 9 × 15 Foot Low Speed Wind Tunnel. (BBN-3176, Bolt, Beranek, and Newman, Inc.; NAS3-19410.) NASA CR-135026, 1976.
7. Diedrich, James H.; and Luidens, Roger W.: Measurement of Model Propulsion System Noise in a Low-Speed Wind Tunnel. AIAA Paper 76-91, Jan. 1976.
8. Dietrich, Donald A.; Heidmann, Marcus F.; and Abbott, John M.: Acoustic Signatures of a Model Fan in the NASA-Lewis Anechoic Wind Tunnel. AIAA Paper 77-59, Jan. 1977.
9. Luidens, Roger W.; and Abbott, John M.: Incidence Angle Bounds for Lip Flow Separation of Three 13.97-Centimeter-Diameter Inlets. NASA TM X-3351, 1976.
10. Motycka, D. L.: Ground Vortex-Limit to Engine/Reverser Operation. ASME Paper No. 75-GT-3, March 1975.

TABLE I. - INLET GEOMETRIC PARAMETERS

Internal lip	
Contraction ratio, $(D_{hl}/D_t)^2$	1.44
Surface contour	Ellipse
Proportions, a/b	2.0
External forebody	
Diameter ratio, D_{hl}/D_{max}	0.85
Ratio of length to maximum diameter, X/D_{max}	0.40
Surface contour	[a]DAC-1
Proportions, X/Y	5.33
Diffuser	
Ratio of exit flow area to inlet flow area, $\left(D_e^2 - D_c^2\right)/D_t^2$	1.048
Ratio of diffuser length to exit diameter, L_d/D_e	0.538
Maximum local wall angle, λ_{max}, deg	8.37
Location of maximum local wall angle, percent L_d	50
Equivalent conical half-angle, deg	1.33
Surface contour	Cubic
Centerbody	
Ratio of centerbody length to diameter, L_c/D_c	1.0
Surface contour	Ellipse
Ratio of centerbody length to diffuser length, L_c/L_d	0.744
Ratio of centerbody diameter to diffuser-exit diameter, D_c/D_e	0.40

[a]The DAC-1 contour was developed by the Douglas Aircraft Co. and is given by

$$\left(\frac{y}{Y}\right)^2 = 2.3176\left(\frac{x}{X}\right) - 2.7485\left(\frac{x}{X}\right)^2 + 2.5437\left(\frac{x}{X}\right)^3 - 1.1131\left(\frac{x}{X}\right)^4.$$

TABLE II. - CIRCUMFERENTIAL VARIATION OF LENGTH FOR SCOOP INLET

Circumferential position, ψ, deg	Ratio of inlet length to diffuser-exit diameter, L/D_e
0	1.295
30, 330	1.290
45, 315	1.266
60, 300	1.207
90, 270	.823
100, 260	.746
105, 255	.727
113.64 to 246.36	.716

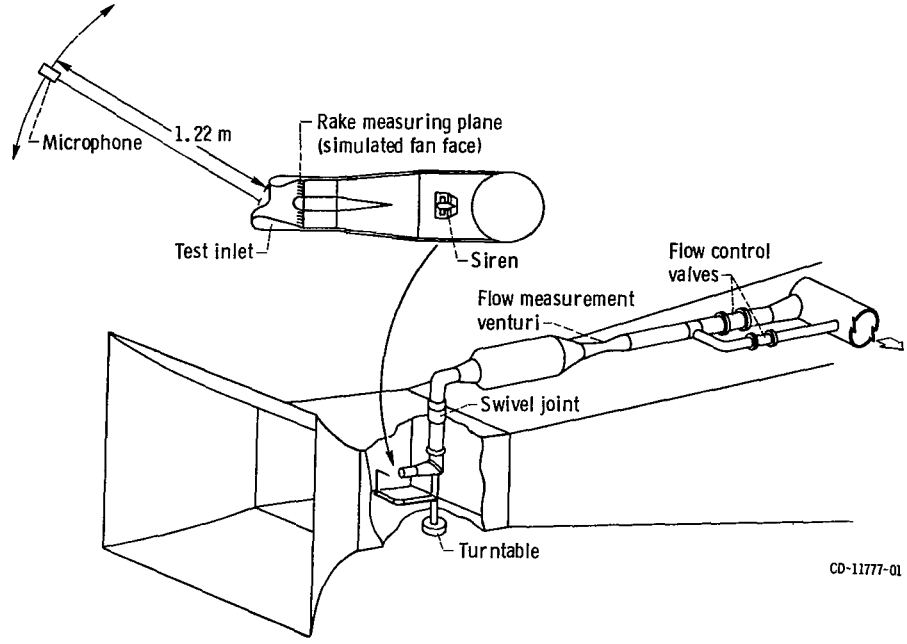

Figure 1. - Schematic of test installation in 2.74- by 4.58-meter (9- by 15-ft) anechoic wind tunnel.

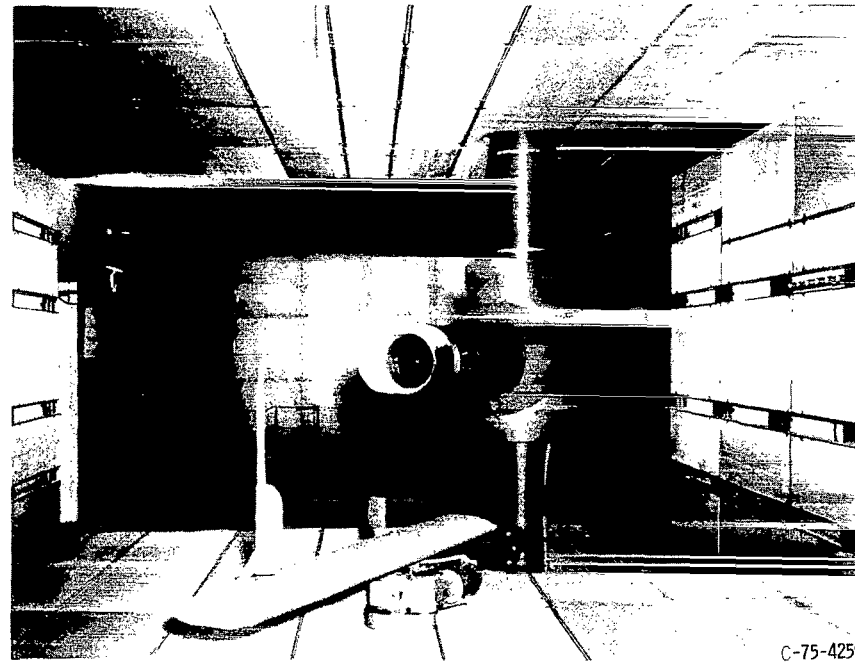

Figure 2. - Test installation in 2.74- by 4.58-meter (9- by 15-ft) anechoic wind tunnel.

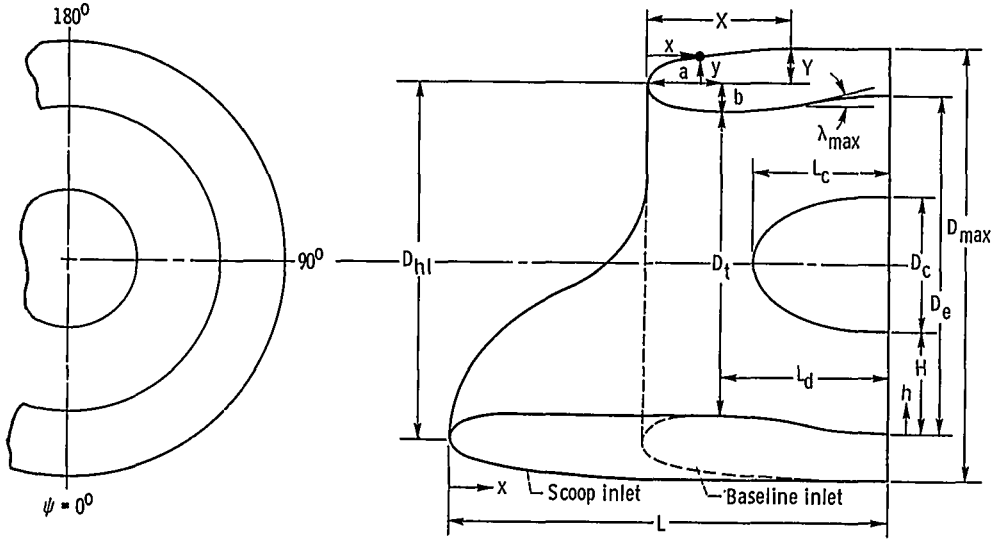

Figure 3. - Inlet nomenclature.

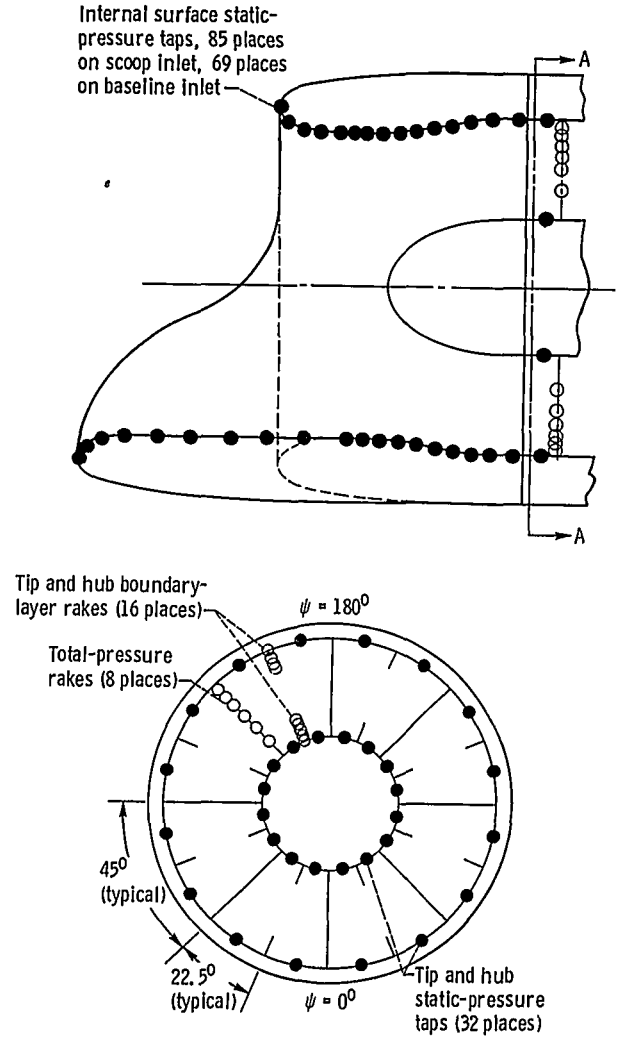

Section A-A (rake measuring plane)

Figure 4. - Instrumentation.

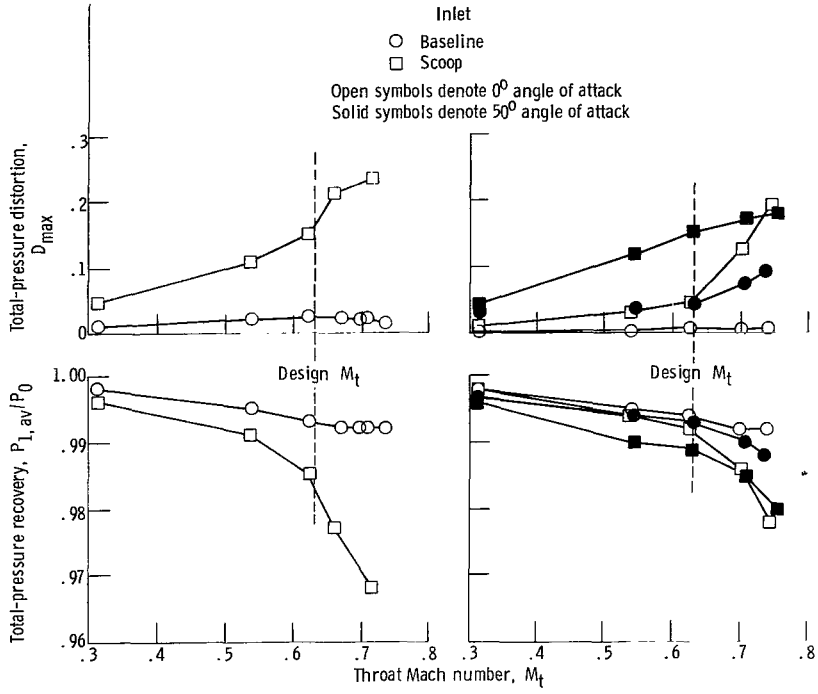

(a) Free-stream velocity, V_0, 0.

(b) Free-stream velocity, V_0, 41 meters per second.

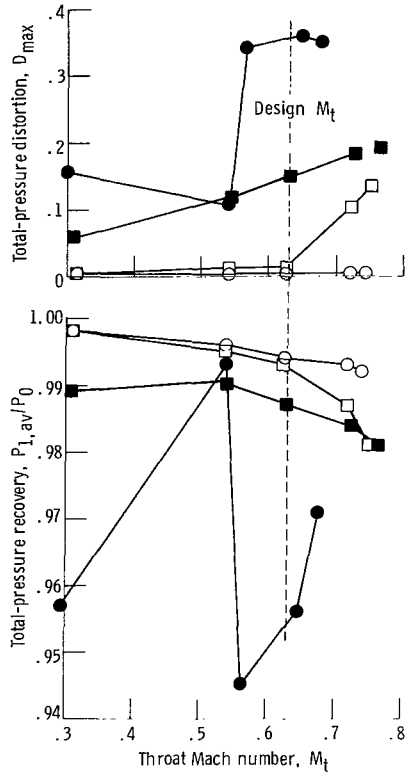

(c) Free-stream velocity, V_0, 61 meters per second.

Figure 5. - Aerodynamic performance of scoop and baseline inlets.

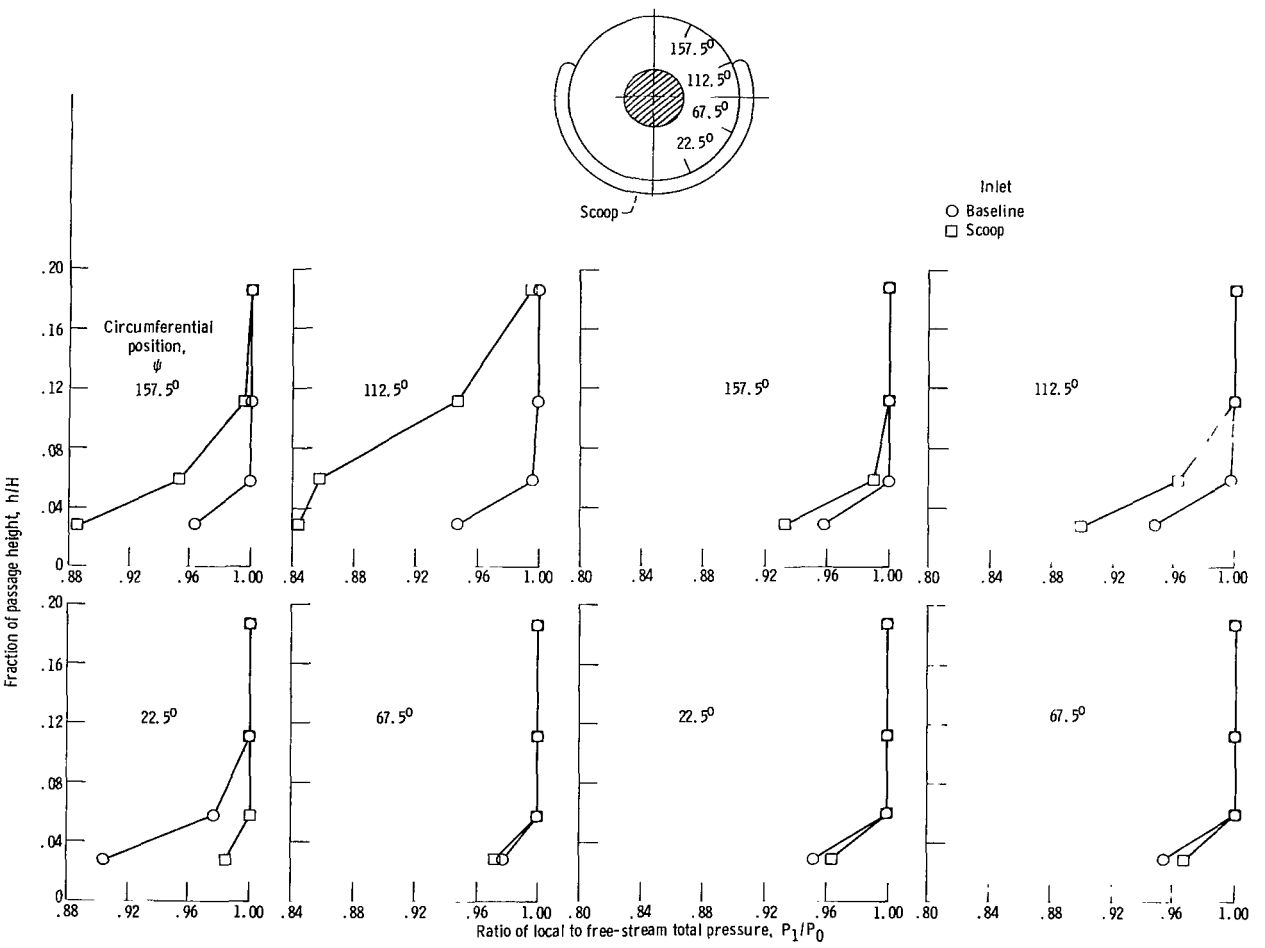

(a) Free-stream velocity, V_0, 0; angle of attack, α, 0^0.

(b) Free-stream velocity, V_0, 41 meters per second; angle of attack, α, 0^0.

Figure 6. - Circumferential total-pressure distribution in tip boundary layer for scoop and baseline inlets. Throat Mach number, M_t, 0.63.

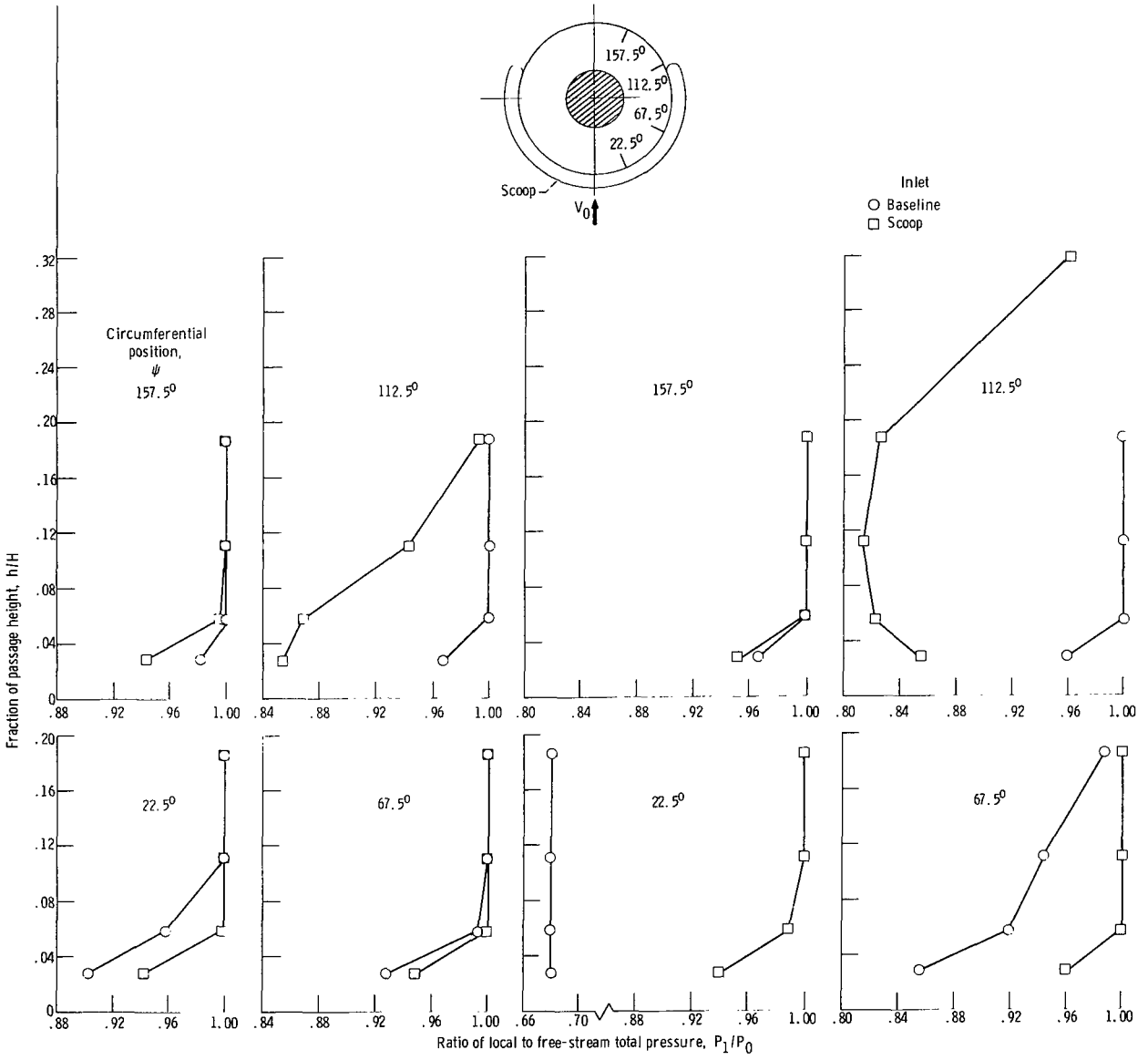

(c) Free-stream velocity, V_0, 41 meters per second; angle of attack, α, 50°.

(d) Free-stream velocity, V_0, 41 meters per second; angle of attack, α, 75°.

Figure 6. - Concluded.

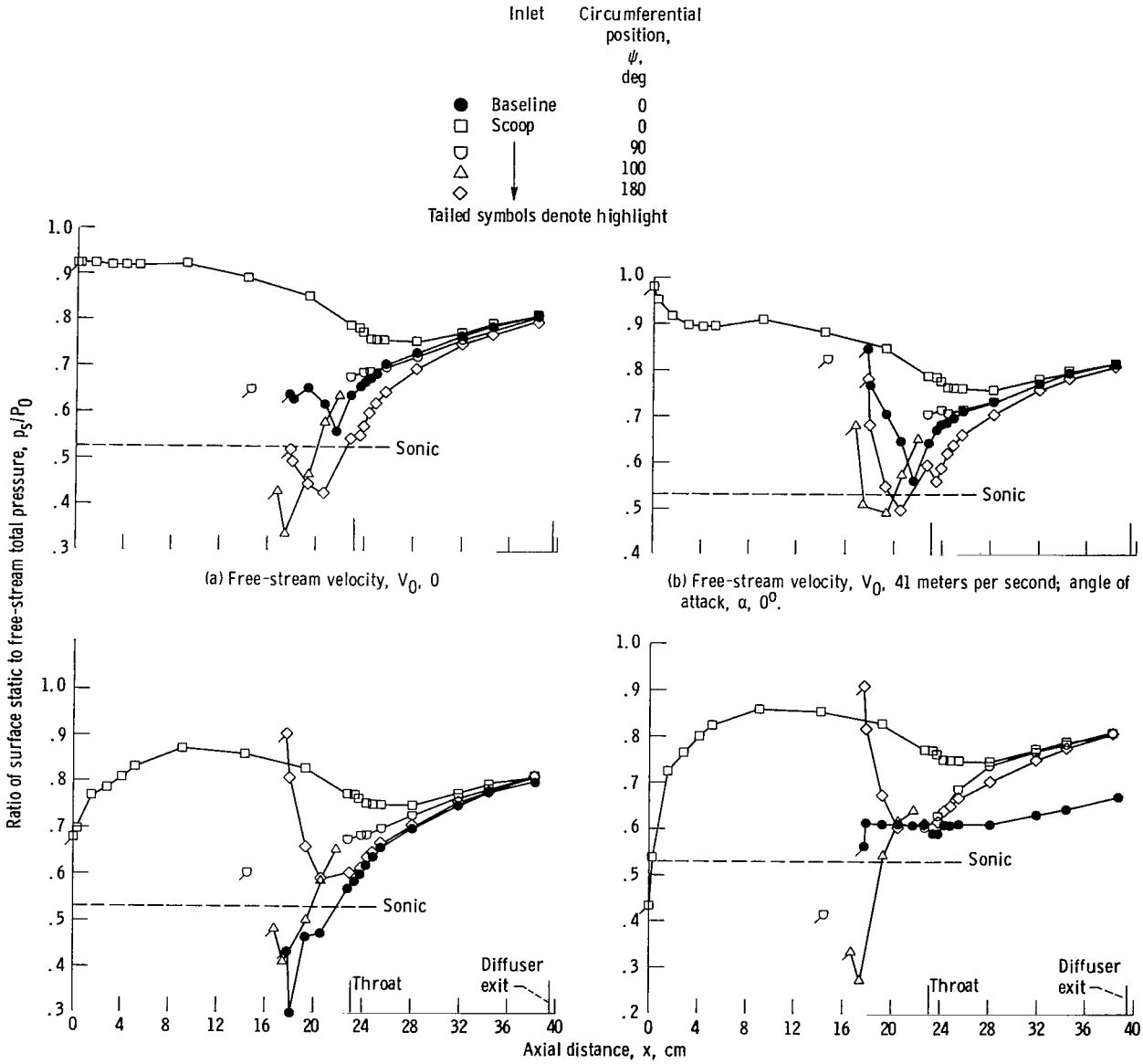

(a) Free-stream velocity, V_0, 0

(b) Free-stream velocity, V_0, 41 meters per second; angle of attack, α, 0^0.

(c) Free-stream velocity, V_0, 41 meters per second; angle of attack, α, 50^0.

(d) Free-stream velocity, V_0, 41 meters per second; angle of attack, α, 75^0.

Figure 7. - Axial distribution of surface static pressure for scoop and baseline inlets. Throat Mach number, M_t, 0.63.

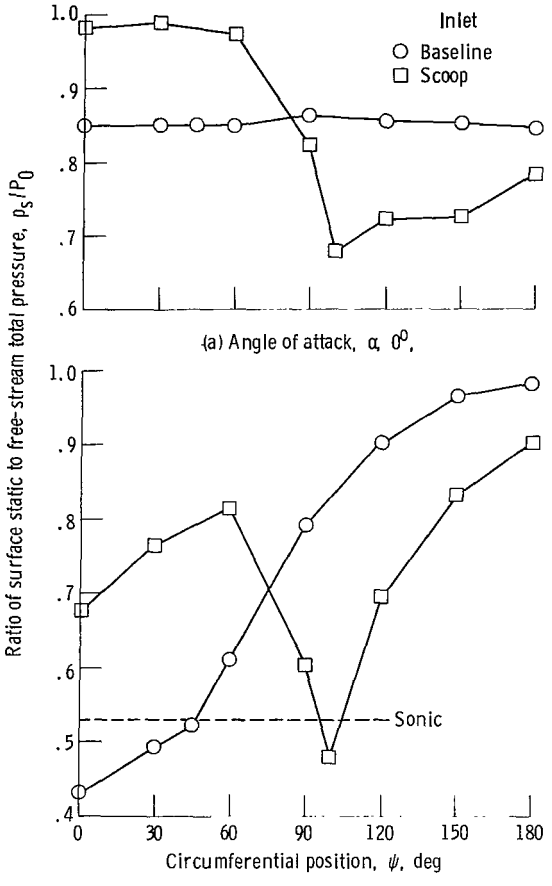

Figure 8. - Circumferential variation of surface static pressure at highlight for scoop and baseline inlets. Free-stream velocity, V_0, 41 meters per second; throat Mach number, M_t, 0.63.

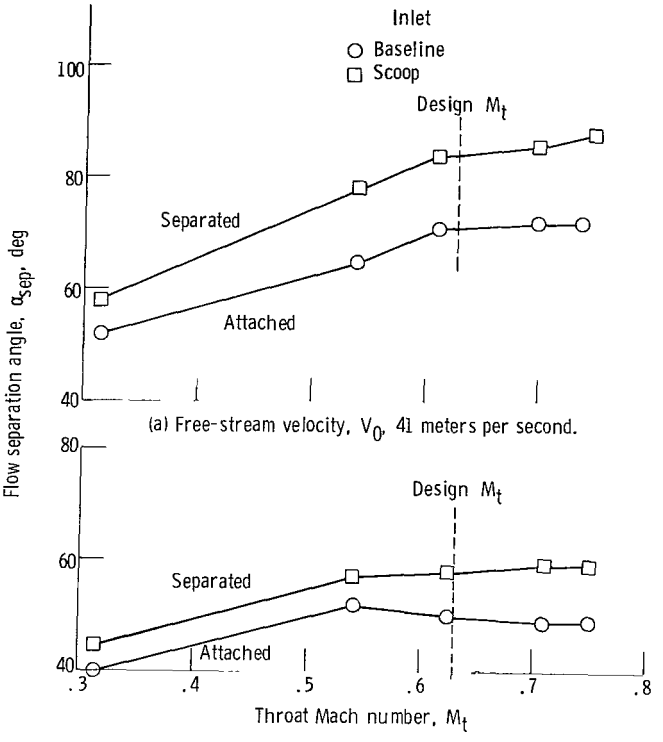

Figure 9. - Flow separation bounds for scoop and baseline inlets.

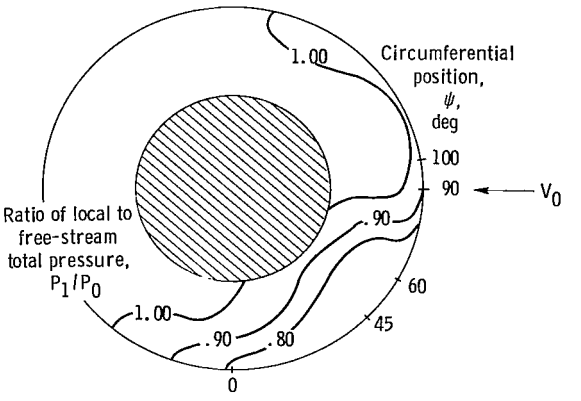

(a) Distribution of total pressure at inlet diffuser exit.

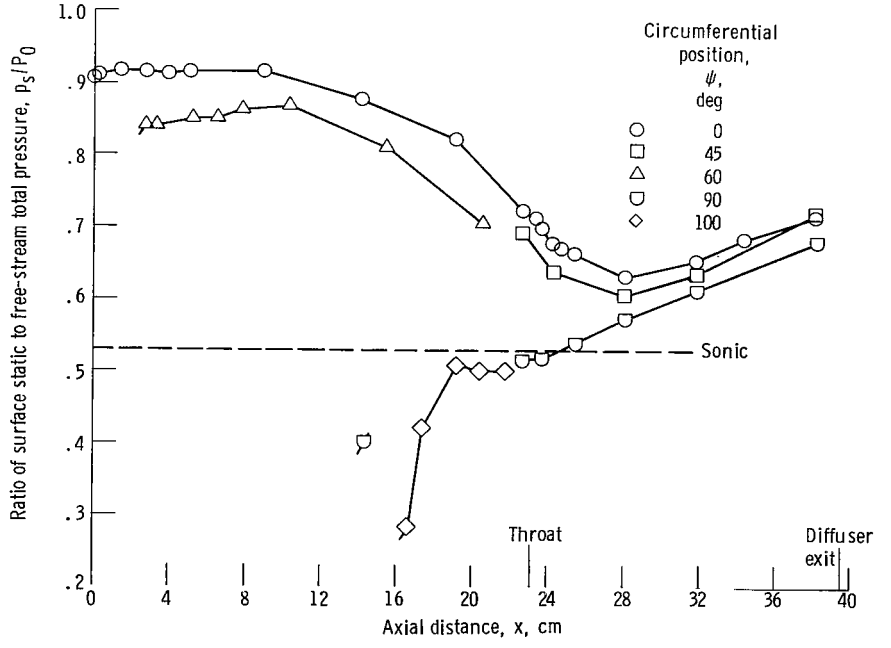

(b) Surface static-pressure distribution.

Figure 10. - Performance of scoop inlet in 90° crosswind. Free-stream velocity, V_0, 18 meters per second; throat Mach number, M_t, 0.63.

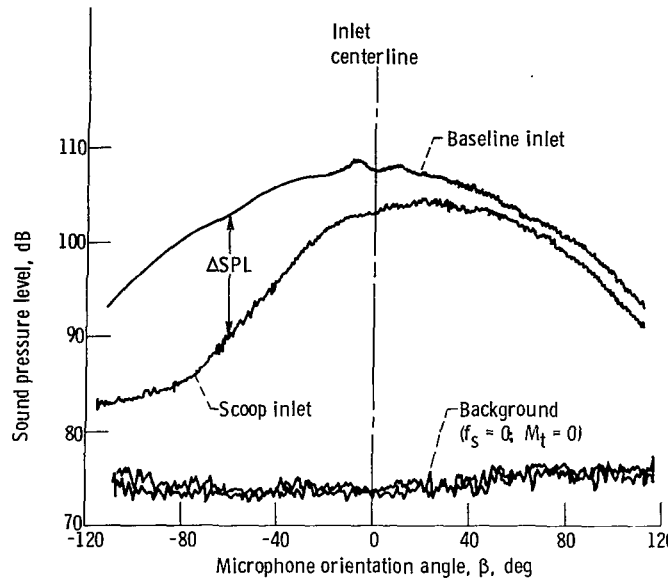

Figure 11. - Comparison of noise directivity for scoop and baseline inlets. Free-stream velocity, V_0, 41 meters per second; angle of attack, α, 0^0; throat Mach number, M_t, 0.63; siren frequency, f_s, 9600 hertz; filter frequency, f_f, 8000 hertz.

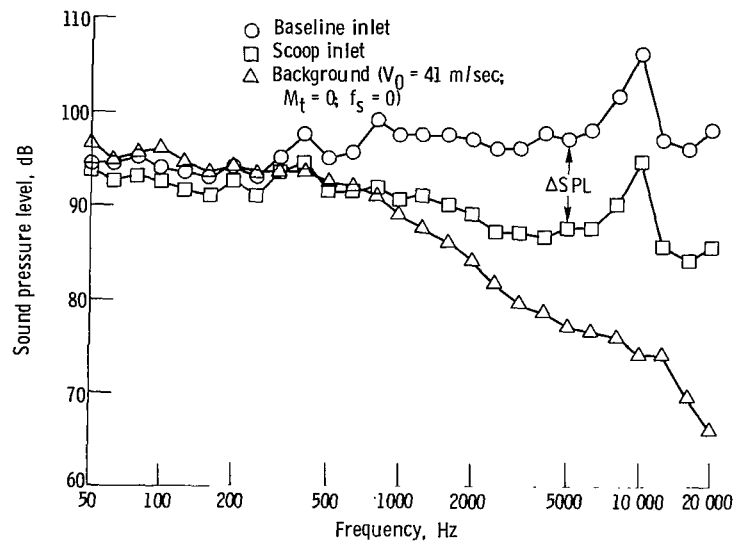

Figure 12. - Comparison of 1/3-octave noise spectra for scoop and baseline inlets. Free-stream velocity, V_0, 41 meters per second; angle of attack, α, 0^0; throat Mach number, M_t, 0.63; siren frequency, f_s, 9600 hertz; microphone orientation angle, β, -60^0.

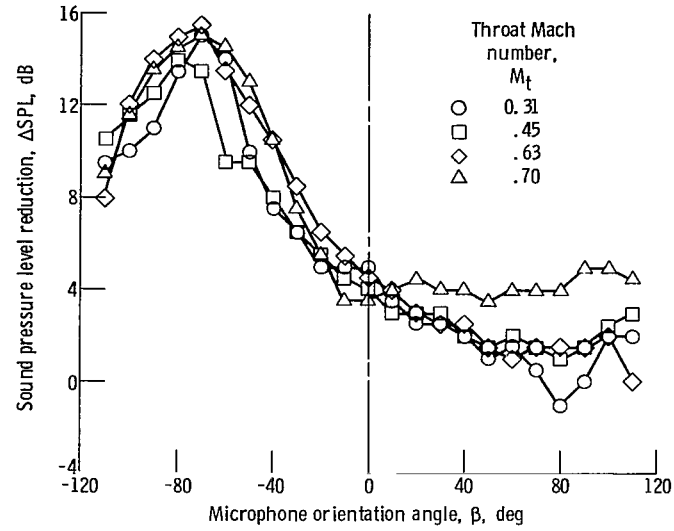

Figure 13. - Effect of throat Mach number on scoop inlet noise reduction. Free-stream velocity, V_0, 41 meters per second; angle of attack, α, 0°; siren frequency, f_s, 9600 hertz; filter frequency, f_f, 8000 hertz.

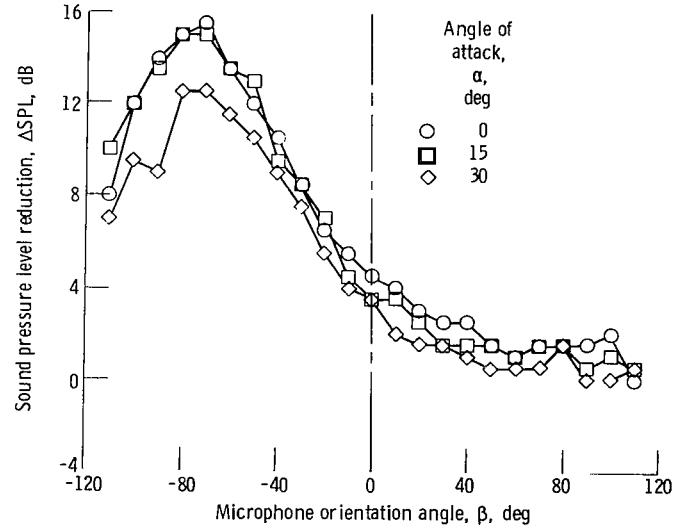

Figure 14. - Effect of angle of attack on scoop inlet noise reduction. Free-stream velocity, V_0, 41 meters per second; throat Mach number, M_t, 0.63; siren frequency, f_s, 9600 hertz; filter frequency, f_f, 8000 hertz.

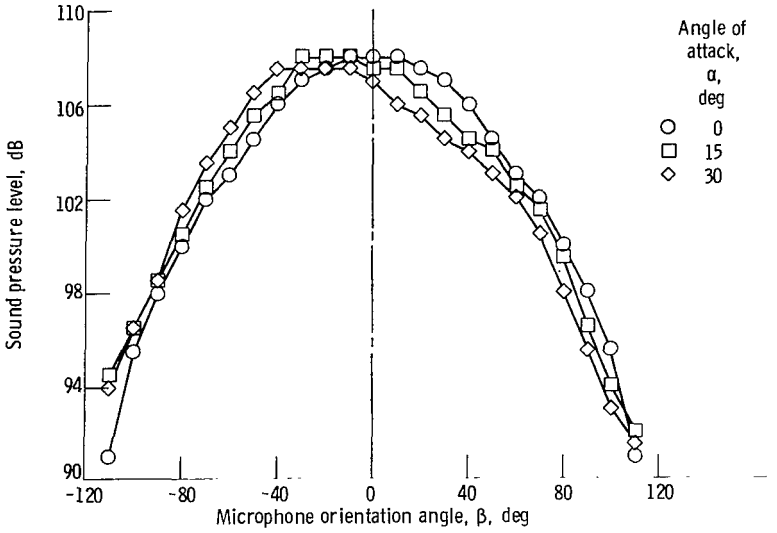

Figure 15. - Effect of angle of attack on baseline inlet noise directivity. Free-stream velocity, V_0, 41 meters per second; inlet throat Mach number, M_t, 0.63; siren frequency, f_s, 9600 hertz; filter frequency, f_f, 8000 hertz.

1. Report No.	2. Government Accession No.	3. Recipient's Catalog No.
NASA TP-1028		

4. Title and Subtitle	5. Report Date
AERODYNAMIC AND DIRECTIONAL ACOUSTIC PERFORMANCE OF A SCOOP INLET	September 1977
	6. Performing Organization Code
7. Author(s)	8. Performing Organization Report No.
John M. Abbott and Donald A. Dietrich	E-9134
	10. Work Unit No.
9. Performing Organization Name and Address	511-54
National Aeronautics and Space Administration Lewis Research Center Cleveland, Ohio 44135	11. Contract or Grant No.
	13. Type of Report and Period Covered
12. Sponsoring Agency Name and Address	Technical Paper
National Aeronautics and Space Administration Washington, D.C. 20546	14. Sponsoring Agency Code

15. Supplementary Notes

16. Abstract

A series of tests was conducted to determine the aerodynamic and directional acoustic performance of a scoop inlet. The scoop inlet is designed with a portion of the lower cowling extended forward to direct upward any noise that is propagating out the front of the engine toward the ground. The tests were conducted in the Lewis anechoic wind-tunnel facility at free-stream velocities of 0, 18, 41, and 61 m/sec and angles of attack from -10° to 120°. Inlet throat Mach number was varied from 0.30 to 0.75. Aerodynamically, at a free-stream velocity of 41 m/sec, the design throat Mach number (0.63), and an angle of attack of 50°, the scoop inlet total-pressure recovery was 0.989 and the total-pressure distortion was 0.15. The angles of attack where flow separation occurred with the scoop inlet were higher than those for a conventional symmetric inlet. Acoustically, the scoop inlet provided a maximum noise reduction of 12 to 15 dB below the inlet over the entire range of throat Mach number and angle of attack at a free-stream velocity of 41 m/sec.

17. Key Words (Suggested by Author(s))	18. Distribution Statement
Inlet design; Scoop inlet; Inlet noise reduction; Inlet noise directivity; Noise refraction; Wind tunnel tests	Unclassified - unlimited STAR Category 07

19. Security Classif. (of this report)	20. Security Classif. (of this page)	21. No. of Pages	22. Price*
Unclassified	Unclassified	27	A03

* For sale by the National Technical Information Service, Springfield, Virginia 22161

NASA-Langley, 1977

587 001 C1 U A 770819 S00903DS
DEPT OF THE AIR FORCE
AF WEAPONS LABORATORY
ATTN: TECHNICAL LIBRARY (SUL)
KIRTLAND AFB NM 87117